Fundamental Research 4 (2024) 1586–1593

Contents lists available at ScienceDirect

Fundamental Research

journal homepage: http://www.keaipublishing.com/en/journals/fundamental-research/

Article

Ice sheet expansion in the Cretaceous greenhouse world

Tianyang Wang[a,b,1,*], Songlin He[a,b,1], Qinghai Zhang[a,b,*], Lin Ding[a,b,*], Alexander Farnsworth[a,c], Fulong Cai[a,b], Chao Wang[a,b], Jing Xie[a], Guobiao Li[d], Jiani Sheng[e], Yahui Yue[a]

[a] State Key Laboratory of Tibetan Plateau Earth System, Environment and Resources (TPESER), Institute of Tibetan Plateau Research, Chinese Academy of Sciences, Beijing 100101, China
[b] University of Chinese Academy of Sciences, Beijing 100049, China
[c] School of Geographical Sciences and Cabot Institute, University of Bristol, Bristol BS8 1SS, UK
[d] School of Earth Sciences and Resources, China University of Geosciences, Beijing 100083, China
[e] School of Earth and Environmental Sciences, University of Queensland, Brisbane 4072, Australia

ARTICLE INFO

Article history:
Received 15 February 2023
Received in revised form 24 April 2023
Accepted 14 May 2023
Available online 26 May 2023

Keywords:
Global carbon-cycle dynamics
Paleoclimatic reconstruction
Clumped and oxygen isotopes
Polar ice volume
Valanginian cooling event

ABSTRACT

Globally elevated temperatures during the Cretaceous extreme greenhouse climate interval were punctuated by the Valanginian cooling event, which was characterized by a positive carbon isotope excursion, global cooling, and a glacial event approximately at 135 Ma. Disentangling ocean temperature and continental ice volume trends enables us to better understand climate fluctuations over deep time. We investigated the ocean temperature–ice sheet dynamics of glaciation events that occurred in the Cretaceous greenhouse world. New clumped isotope and $\delta^{18}O$ data from sites in the Tethyan Ocean show that seawater temperatures decreased by 5–6 °C, consistent with the development of glacial periods, and maximum ice volumes about half the size of present-day Antarctica. This cooling event provides a counter-example to other Mesozoic climate transitions driven by changes in atmospheric greenhouse gas contents. Our results emphasize the importance of quantitatively reconstructing continental ice volume, providing further support for exploring deep-time Earth climate dynamics.

1. Introduction

Paleoclimate reconstructions reveal variable and complex conditions in the Cretaceous on the basis of geochemical results and climate models [1–3]. Geochemical proxies such as the organic paleothermometry TEX_{86} and planktonic foraminiferal $\delta^{18}O$ suggest the Early Cretaceous long-term greenhouse conditions were disrupted by Valanginian and Aptian cooling events [4–6]. The Valanginian episode (i.e., the Weissert event) was characterized by a positive carbon isotope excursion (CIE) [7,8], and may represent a dynamic interval of temperature variations [9,10], decreased atmospheric pCO_2 [10,11], sea level fall [12–14], and potential formation of polar ice sheets [10,15,16]. Indeed, the occurrence of rapid sea level change and global cooling trends over short timescales, coupled with physical evidence for southern hemisphere glaciation, suggests that glacio-eustasy played a role during this episode [17–19]. In other words, arguments in favor of Valanginian glacial events rely on polar regions closer to freezing [15], sequence stratigraphy [12], glaciogenic features [19], and positive seawater $\delta^{18}O$ values [20]. Late Valanginian atmospheric pCO_2 declines were lower than previous climate modeling results [9,10], adding support for the existence of a polar ice sheet. However, the nature, magnitude, and frequency of these climatic fluctuations are unclear, which limits our understanding of the coupling of seawater temperatures and ice volume during the greenhouse-to-coolhouse (ice-free to ice sheets) transition in the Early Cretaceous.

Stable oxygen isotopic compositions of marine fossil shells provide constraints on the growth and demise of continental ice volumes [21]. A positive shift of $\delta^{18}O$ values suggests accumulation of ice volumes and sea level decline [22]. However, this proxy is not perfect to reconstruct ice volumes because $\delta^{18}O$ values also reflect seawater temperature changes and local variables, such as salinity and seawater pH [5]. Reconstructing ancient sea temperatures from high-resolution sedimentary records is the most direct way to examine secular trends in past climate. Carbonate clumped isotope (expressed with the parameter Δ_{47}) paleothermometry is an important method for reconstructing past temperatures [23]. This proxy is based on the preference for ^{13}C and ^{18}O to bond with each other in the carbonate molecule, which is an effect that becomes more prominent with decreasing temperatures [24,25]. An important distinction between clumped isotope and conventional $\delta^{18}O$ thermometry is that the former does not depend on the isotopic composition of the aqueous phase from which the carbonates form, and is based on isotope exchange reactions within a single mineral phase [25,26]. As

* Corresponding authors.
E-mail addresses: wangtianyang@itpcas.ac.cn (T. Wang), zhang@itpcas.ac.cn (Q. Zhang), dinglin@itpcas.ac.cn (L. Ding).
[1] These authors contributed equally to this work.

https://doi.org/10.1016/j.fmre.2023.05.005

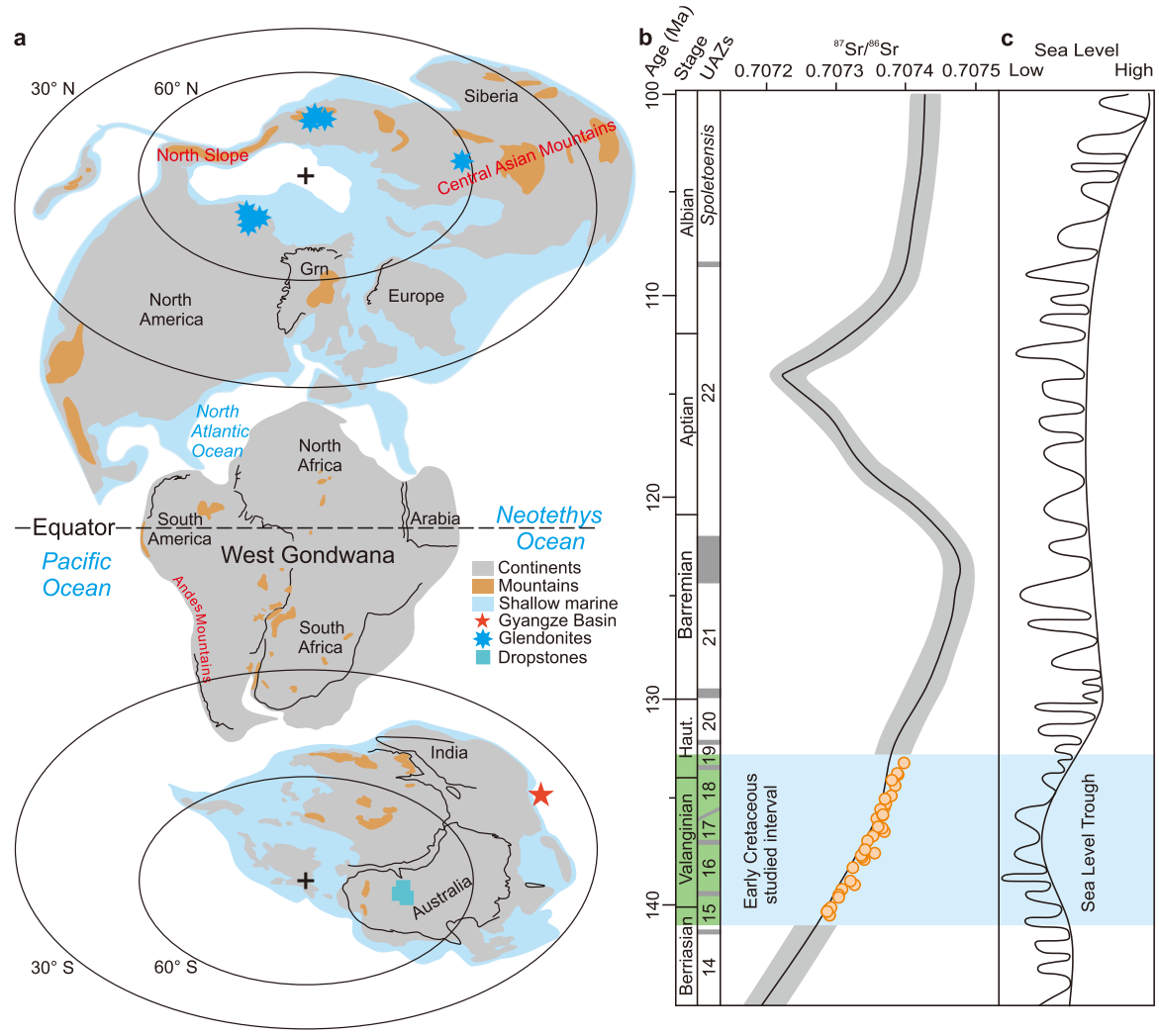

Fig. 1. Early Cretaceous paleogeography and $^{87}Sr/^{86}Sr$ and sea level curves. (a) Locations of the sample sections and glacial evidence [17,19] shown on a paleogeographic map (after ref. [11]). (b) Estimated numerical age of the study interval obtained using the $^{87}Sr/^{86}Sr$ seawater values and the LOESS look-up table [16,29], with gray shading representing the 1 SD uncertainty range. (c) The eustatic sea level changes of Haq [12]. Note the Weissert event coincides with the lowest sea level of the Cretaceous because of glacio-eustasy.

such, clumped isotope thermometry of measured carbonate should only depend on the thermodynamic equilibrium formation temperature of the carbonate, making it an ideal tool for reconstructing paleoclimatic conditions over deep time [24,26].

In this study, we investigate the coupling of global carbon cycling, Southern Hemisphere seawater paleotemperatures, and sea level changes using clumped isotope thermometry, stable isotope and trace element data for well-preserved belemnite rostra from the shale layers of the Gyabula Formation in the Gyangze Basin, southern Tibet. The Gyangze Basin is known to have been a marginal marine basin that formed near the Indian continent and was constrained to a paleolatitude of approximately 45°S using paleomagnetic and geochronological data from Early Cretaceous lava flows in the Tethyan Himalaya [27] (Figs. 1a and S1). Low-Mg calcite rostra of belemnites, which are extinct coleoid cephalopods, are widely distributed in Mesozoic marine sediments. Although evaporation and weathering inputs may affect the $\delta^{18}O$ values of belemnite calcite and seawater, our study area is thought to have been an open marine environment based on the presence of a fully marine fauna [28]. Therefore, any effects from these processes on our calculations would have been minimal. Samples that lack evidence of petrographic and geochemical alteration were analyzed and are considered to retain the primary carbonate chemistry according to our assessment methods (*Materials and Methods*). Our multiproxy approach suggests that reconstructing mid-latitude Tethyan Ocean temperatures and sea level fluctuations during the Valanginian episode provides a better understanding of the climate forcing and feedbacks that related to glacio-eustatic processes. This includes environmental change, perturbations in the global carbon cycle, and the growth and demise of ice sheets in a greenhouse climatic system.

2. Materials and methods

2.1. Assessment of belemnite rostrum

We collected over 200 belemnite rostra samples from three Lower Cretaceous sections in southern Tibet: Qiabu (28.85372°N, 89.83472°E), Longma (28.89722°N, 89.94444°E), and Manla (28.83528°N, 89.88806°E), primarily corresponding to *Hibolithes* but less commonly to *Belemnopsis* and *Duvalia*. To eliminate the effects of interspecies variability, we collected multiple specimens from the same bed whenever possible. We assessed the preservation of the rostra through various methods, including petrographic observations, cathodoluminescence (CL) microscopy, scanning electron microscopy backscattered electrons (SEM-BSE), and electron probe micro-analysis (EPMA) elemental mapping of polished thick-sections of the belemnites. The SEM-BSE and CL microscopy were conducted at the State

Key Laboratory of Biogeology and Environmental Geology of China University of Geosciences, Beijing, using a Zeiss Supra 55 SEM and a Cambridge Image Technology Limited Cl8200mk5 electron source, respectively. EPMA was performed with a JOEL JXA-8230 electron microprobe at the State Key Laboratory of Tibetan Plateau Research Earth System, Environment and Resources (TPESER), Institute of Tibetan Plateau Research, Chinese Academy of Sciences (ITPCAS). After imaging, we took approximately 500 mg of powdered sample from each well-preserved region of the rostra using a handheld dental drill with low speed. We measured levels of calcium, magnesium, strontium, iron, and manganese concentrations using a solution method with a Thermo X Series inductively coupled plasma-mass spectrometer (ICP-MS) at TPESER, ITPCAS.

2.2. Conventional stable isotope analysis

Stable isotope analyses were performed on approximately 300 μg of powdered calcites at the Laboratory for Stable Isotope Geochemistry, Institute of Geology and Geophysics, China Academy of Sciences, Beijing, China and were performed by a mass spectrometer (Thermo Fisher Scientific MAT 253) coupled to a Gas bench II preparation system. The analytical precision was better than ± 0.15‰ for $\delta^{13}C$ and ± 0.20‰ for $\delta^{18}O$, based on replicate analyses of the NBS 19 carbonate international standard. All isotope ratios are presented in per mil (‰) related to the Vienna Pee Dee Belemnite (VPDB) standard.

2.3. Strontium isotope stratigraphy

$^{87}Sr/^{86}Sr$ ratios were measured after Sr separation from other elements in the belemnite rostrum by cation exchange chemistry using AG50W-X4 resin. The $^{87}Sr/^{86}Sr$ ratios were measured with a Nu Plasma II multi-collector ICP-MS at the State Key Laboratory of Tibetan Plateau Earth System, Environment and Resources, Institute of Tibetan Plateau Research, Chinese Academy of Sciences, Beijing, China. For biogenic calcite, 1–3 mg of powdered sample is needed. The NIST SRM 987 international Sr standard was used to assess the instrumental stability. Total procedural blanks were 300 pg for Sr. Data were normalized to the mean value of 0.710248 ± 13 (2 SD; n = 41) for SRM 987. Measured $^{87}Sr/^{86}Sr$ ratios were normalized to $^{86}Sr/^{88}Sr = 0.1194$ to correct for mass fractionation. The long-term reproducibility (2 SD) was < ± 0.000010 for routine analyses. The $^{87}Sr/^{86}Sr$ ratios were projected onto the global marine $^{87}Sr/^{86}Sr$ calibration curve (Look-up Table) [29] to obtain numerical ages (Fig. S6; Tables S1–S3).

2.4. Clumped isotope thermometry

We undertook carbonate clumped isotope analyses in the newly established experimental systems at the State Key Laboratory of Tibetan Plateau Earth System, Environment and Resources, Institute of Tibetan Plateau Research, Chinese Academy of Sciences, Beijing, China. To facilitate accurate seawater paleotemperature calculations, we have assessed the preservation state of each analyzed sample using visual and geochemical methods mentioned earlier in this study. Twenty-nine well-preserved belemnite rostra of *Belemnopsis* (n = 2) and *Hibolithes* (n = 27) from the Lower Cretaceous Gyabula Formation deposits in the southern Tethys were analyzed to estimate the formation temperature of the biogenic calcite. Powder samples (5.5–6.5 mg) were digested using 1 mL anhydrous phosphoric acid (specific gravity = ~1.93 g/cm^3, ~104%) in a common acid bath at 90 °C for 15 minutes. After acid digestion, the generated CO_2 samples were then purified off-line before entering a MAT 253plus gas source isotope ratio mass spectrometer to obtain the raw Δ_{47} data. To convert the carbonate formation temperatures [$T(\Delta_{47})$], we use the thermometry of Kele et al. [30] calibration, which was recalculated with the "Brand parameters" and new accepted values for the ETH standards, as reported in Bernasconi et al. [31], owing to its similar sample type and extensive temperature coverage. All the raw data and detailed laboratory methods are provided in the Supplementary materials.

$$\Delta_{47} = 0.0449(\pm 0.001) \cdot \frac{10^6}{T^2} + 0.167(\pm 0.01) \quad (1)$$

where T is the temperature in Kelvin. In an open marine setting, this equation represents equilibrium fractionation between calcite and water and yield $\delta^{18}O_{sea}$ values within the expected range [32].

3. Results and discussion

3.1. Belemnite paleoecology, preservation, and selection

Low-Mg calcite rostra of belemnites are valuable geochemical archives for paleoenvironmental studies. Previous results have also inferred that the isotopic compositions ($\delta^{18}O$ and Δ_{47}) of well-preserved belemnite calcite can be used to interpret environmental parameters of the seawater in which they lived [9,20,32]. The $\delta^{18}O$ of benthic foraminifers and the TEX_{86} methods are thought to calculate deep ocean water temperatures and sea surface temperatures (SSTs), respectively. Belemnites, as both predators and prey, typically inhabit the epipelagic zone for only 1–2 years, with limited movement below 200 m of the water column because of the presence of very thin aragonitic phragmocone septa and wall [33]. Interestingly, *Hibolithes* with elongate and slender rostra were probably nektic and fast swimmers that undertook vertical migration in the water column [33]. It is therefore thought that the geochemical results from belemnite calcite $\delta^{18}O$ and Δ_{47} measurements primarily reflect mean annual seawater signals from the thermocline layer (< 200 m).

Based on the petrographic and geochemical methods employed, the results for the interpretation of well-preserved rostrum calcite include the following observations: optical inspection reveals no observable larger cracks or dissolution features (Fig. S2). Most regions of the studied rostra exhibit blue to dark luminescence under CL (Fig. S2e, 2f), which is indicative of unaltered material and matches the intrinsic CL color of calcite [15]. SEM-BSE images demonstrate radiaxial fibrous calcites increasing in width and length from the centra towards outer rim, which is in agreement with published SEM observations on well-preserved belemnite fossils [32] (Fig. S3). Additionally, electron microprobe elemental maps indicate uniformly low Mn and Fe contents with compositional changes in S and Mg occurring in the growth rings of the rostra (Fig. S3). The variations in S and Mg beyond the apical area during the progressive growth and calcite precipitation of the belemnite rostra are attributed to organic compounds incorporated into the carbonate biominerals, signifying biomineralization rather than diagenetic processes [32]. Furthermore, ICP-MS analysis suggests that the well-preserved belemnite calcite contains relatively low concentrations of Mn (< 30–50 μg/g) and Fe (< 150 μg/g) [16,20] (Figs. S3, S4; Tables S1–S3). Previous geochemical investigations of modern and fossil Mollusca have shown that primary biominerals have low concentrations of Mn and Fe, with diagenetic alteration causing the enrichment of these two elements in biogenic carbonates [29]. Out of the 131 belemnite rostra samples analyzed, 116 were determined to be unaltered biogenic carbonate and therefore suitable for paleoclimate interpretations. Stable isotopic results of these unaltered belemnite rostra reveal that there is no significant correlation between the $\delta^{13}C$ and $\delta^{18}O$ ratios (Fig. S4). This observation supports that paleoenvironmental interpretation is possible [34]. In addition, burial of sediments was limited to a maximum of 700 m in the studied localities. We can therefore estimate that burial temperatures did not exceed 75 °C in these sediments and that solid-state reordering did not affect Δ_{47} values of belemnite rostra found in these succession [35].

3.2. Biostratigraphy and strontium and carbon isotope stratigraphy

The radiolarian biostratigraphy used in this study is detailed in Fig. S5, which is based on the unitary association zones (UAZs). The up-

permost Berriasian to lower Valanginian part of the studied marine succession is well constrained by the occurrence of *Thanarla pulchra*, which characterizes UAZ 15 in the Tethyan realm. Although radiolarians are less common, the interval of UAZ 16 is correlated with the co-occurrence of *Acaeniotyle umbilicata, Godia* sp., and *Pantanellium squinaboli*, and is assigned to the lower Valanginian. Previous studies of the evolution of Early Cretaceous radiolarians in the western Tethys have shown that positive CIE excursions coincide with the increase in the abundance of upwelling, high productivity-related *Pantanellium* during the upper Valanginian interval [7]. In the Manla section, the increase in abundance of *Patanelliun squinaboli*, along with the co-occurrence of *Hemicryptocapsa capita*, is interpreted to be the upper Valanginian interval. The base of the Hauterivian was placed at the base of UAZ 19 and is defined by the first occurrence of *Cecrops septemporatus*, which is a common specie in the Tethyan realm (Fig. S5).

While the radiolarian biostratigraphy provides relatively high resolution and is consistent with the Tethyan ammonite zones within approximately 9 million years, Sr isotope data can offer significantly improved geochronological resolution. The $^{87}Sr/^{86}Sr$ isotope curve through the studied succession matches that of the uppermost Berriasian to lower Hauterivian interval, which was characterized by seawater Sr isotopic homogeneity in the Early Cretaceous. The belemnite $^{87}Sr/^{86}Sr$ ratios are characterized by increasing values from 0.707286 ± 0.000007 in the lowermost UAZ 15 to 0.707398 ± 0.000006 in the lower UAZ 19, which yields ages of 140.41 ± 0.33 Ma to 133.46 ± 0.19 Ma based on the LOWESS model [16,29], respectively. Our new stratigraphic sections of the Lower Cretaceous Gyabula Formation have tight chronological constraints based on the radiolarian and ammonite biostratigraphy and high-resolution $^{87}Sr/^{86}Sr$ isotope data (Figs. 1 and S6), which allows these sections to be used for stratigraphic correlations and constraining global paleoenvironmental changes through time.

The carbon isotope values of belemnite calcite ($\delta^{13}C_{bel}$) throughout the studied succession range from −2.03‰ to 0.73‰. Our studied sections exhibit near uniform secular trends consistent with global carbon isotopic stratigraphy, and can be divided into four successive intervals according to offsets in $\delta^{13}C_{bel}$ values (Fig. 2; Tables S1–3). In the pre-CIE interval, the $\delta^{13}C_{bel}$ data are derived from the genera *Belemnopsis* and *Hibolites*, and exhibit slight variations about an average value of −1.64‰ ± 0.30‰ (n = 31) during the lower to middle UAZ 16. This rather stable period is interrupted by a large positive CIE that lasted ca. 0.5 Myr, which is known as the onset of the Weissert CIE. The main phase of the CIE is characterized by a positive shift and the highest $\delta^{13}C_{bel}$ values (+0.73‰) in the bottom of UAZ 18. From UAZ 18, the $\delta^{13}C_{bel}$ data tend to delineate a distinct negative excursion up to the top of the sequence, and were mainly derived from the genus *Hibolites*.

3.3. Belemnite carbon isotope records and correlation with the global Weissert event

Our $\delta^{13}C_{bel}$ data suggest that a major positive CIE is evident from the belemnite calcite data in the southern Tethyan Ocean, which is consistent with bulk organic carbon (C_{org}) and carbonate (C_{carb}) data for the northern Tethyan Ocean [8], Boreal Realm [36], western North Atlantic Ocean [37], and Pacific Ocean [7], including shallow marine, hemipelagic, pelagic, and continental settings (Fig. S7 and Table S4). In the southern Tethyan Ocean (ca. 53°S), $\delta^{13}C$ values of bulk carbonate show long-term variations between −2.5‰ and 1.5‰ [36]. This variation of 4‰ is larger than the Valanginian (2.5‰) documented by belemnite calcite data from southern Tibet (ca. 45°S; this study). In the Northern Hemisphere, where the stratigraphic records and geochemical data for belemnite calcite are near complete, a minimum $\delta^{13}C_{bel}$ value at the base of the lower Valanginian is followed by a pronounced increasing trend in the lower part of the upper Valanginian [36]. The major $\delta^{13}C_{bel}$ excursions of ca. 0.5‰ and 1.9‰ above the base of the *S. verrucosum* zone in Spain have been correlated to peaks at a similar stratigraphic level in France (i.e., the northern Tethyan Ocean). These

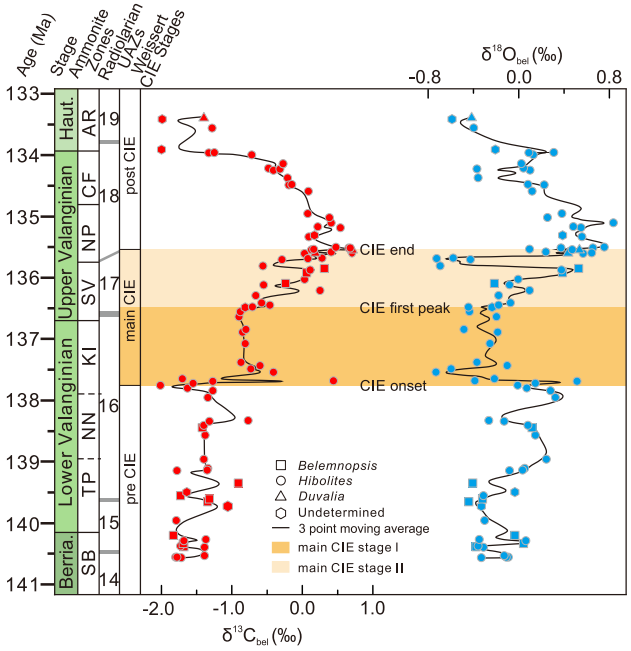

Fig. 2. The carbon and oxygen isotopic trends recorded by belemnites rostra are presented in this study. (a) $\delta^{13}C$ values of belemnites rostra from the Tethyan Ocean, reported in per mil (‰) relative to Vienna PeeDee Belemnite (VPDB). The different Weissert carbon isotope excursion (CIE) stages, including pre-CIE, main CIE and post-CIE, have been identified through the correlation of worldwide $\delta^{13}C$ stratigraphy as shown in Fig. S7. The main CIE has been divided into two stages based on the boundary of CIE onset, CIE first peak, and CIE end. (b) $\delta^{18}O$ values of belemnites rostra from the Tethyan Ocean, reported in per mil (‰) relative to VPDB. The timescale used in this study is based on reference [29].

$\delta^{13}C_{bel}$ maxima can also be correlated to studied sections in Germany and England (i.e., the southern Boreal realm) and Russia (i.e., the Arctic Boreal realm) [7,36,38], where similar positive excursions are found in the middle of the *P. hollwedensis* and *D. crassus* zones, respectively (Fig. S7). Comparison of the belemnite isotope curves for these different regions suggests that the $\delta^{13}C_{bel}$ data exhibit similar long-term trends, but differences in the amplitudes of excursions and absolute values, which may be explained by the biogeographic separation of the sites and preservational and/or taxonomic characteristics. The Valanginian belemnite assemblages exhibit distinct regionality, and can be attributed to two biogeographic realms, which are the Boreal and Tethyan realms. The stable isotope data for the Boreal realm are mainly from the genera *Arctoteuthis, Cylindroteuthis*, and *Lagonibelus*, while the Tethyan data are mainly from *Belemnopsis, Castellanbelus, Duvalia*, and *Hibolithes* [39].

Belemnite and bulk marine carbonate were affected by externally derived carbon during the Weissert event, including carbonate platform- and terrestrial-derived dissolved inorganic carbon (DIC), atmospheric CO_2, and/or methane [8,10,40]. The different magnitudes of the CIE in the bulk marine and belemnite carbonate have previously been explained by the different habitat distributions of coccolithophores and belemnites, which broadly represent the epipelagic and bathypelagic DIC pools, respectively [41]. Moreover, our clumped isotope-derived temperatures, along with other studies of belemnite rostra, suggest that the belemnites lived in deeper and colder waters than indicated by TEX_{86} records. In the Wawal core, a CIE of 2.2‰ recorded by the benthic foraminifer *Lenticulina* reflects the change in deep-ocean DIC [42], which is similar to the median magnitudes of the CIE obtained from the belemnite rostra (2.4‰) (Table S4). In contrast to coccolithophores, belemnites were predators that hunted small-sized faunas beneath the epipelagic zone. A different vertical distribution of these two faunas is

therefore can be used to explain the different magnitudes of the CIE recorded by bulk marine and belemnite carbonate [8,41]. Given that most exogenic carbon is stored as DIC in the marine water column [43], our $\delta^{13}C_{bel}$ data reflect the dynamic coupling of the oceanic carbon pool and global carbon cycling. A major positive CIE in both continent and ocean could have contributed to the observed late Valanginian decrease in atmospheric pCO_2 [10,11], regardless of the precise mechanism.

3.4. Reconstruction of seawater temperatures and $\delta^{18}O$ values

Global climatic perturbations have been previously documented across the Valanginian interval by oxygen and clumped isotope [15,16,20], TEX_{86} [9,10], and Mg/Ca paleothermometries [16]. This decrease in seawater temperature is also recorded by our Δ_{47} values for the belemnite rostra (Figs. 3 and 4). The belemnite Δ_{47} values vary between 0.662 ± 0.012‰ and 0.698 ± 0.010‰, and yield seawater temperatures of 17.7 ± 2 °C to 28.2 ± 2 °C (Table S5). This range of Δ_{47} values can be attributed to seawater temperature fluctuations recorded by the belemnite rostra. Based on the dual clumped isotope analysis (Δ_{47} and Δ_{48}) of a single belemnite rostrum, clumped isotope close to equilibrium formation of belemnite calcite has been proved [44]. The temperatures are also consistent for a variety of taxa, indicating there are no significant intra-specific vital effects. Our data reveal there was a long-term stable climate condition in the pre-CIE interval and an abrupt temperature increase of 3–4 °C at the onset of the CIE interval. This abrupt warming was interrupted by an additional cooling of 4.9 °C, which corresponds to a total temperature decrease of 6 °C that lasted for < 2.4 Myr in response to the Valanginian cooling event (Fig. 4). In addition, the entire Δ_{47} record for the main phase of CIE is suggestive of cooler conditions, although a few samples have lower Δ_{47} values suggestive of short-lived warming events within a much cooler interval. Our data also show that average seawater temperatures (24 °C) for the Valanginian cooling event at mid-latitudes (45°S) are lower than the average BAYSPAR-derived SSTs of ca. 27.8 °C for the Weddell Sea (54°S) [10] and global-average TEX_{86}^{H}-derived SSTs of ca. 35 °C [2]. The discrepancy between the reconstructed seawater temperatures from TEX_{86} and those derived from Δ_{47} values of belemnite calcite may be attributed to the seasonality and vertical migration of belemnites within the thermocline layer [9,41].

The recorded $\delta^{18}O_{bel}$ values throughout the studied succession fluctuate around 0.0‰. Starting with values of about −0.3‰ in the lowest UZA 15, there is a slight increase of about 0.3‰ up to the upper part of UAZ 16. A progressive warming interval between the *K. inostranzewi* and *S. verrucosum* zones is characterized by average $\delta^{18}O_{bel}$ values that are slightly negative at the onset of the Valanginian CIE, and then increase abruptly to ca. 1‰ in the *N. peregrinus* zone. In the southern Tethyan Ocean (ca. 45°S), $\delta^{18}O_{bel}$ values increase steadily towards a maximum of +0.81‰ in UAZ 18 above the Valanginian CIE at approximately the *S. verrucosum–N. peregrinus* boundary. Thereafter, $\delta^{18}O_{bel}$ values decrease by approximately 0.6‰ up to the top of UAZ 18 and remain relatively uniform at 0‰ up to the Valanginian–Hauterivian boundary. In addition, our seawater temperatures and the equilibrium relationship of Kele et al. [29] between temperature and $\alpha_{cc/w}$ allow the $\delta^{18}O$ of the fluid that the inorganic calcite formed in to be determined. Changes in the oxygen isotopic composition of seawater [$\delta^{18}O_{sea}$, relative to Vienna standard mean ocean water (VSMOW)] are ca. 2‰ (−1.3‰ to 0.4‰) (Table S6), based on the $\delta^{18}O_{bel}$ values of −0.73‰ to 0.62‰ and temperatures of 17.7 °C to 28.2 °C.

3.5. Implications for Early Cretaceous ice sheets

Multiple proxies have revealed oceanic cooling and positive CIEs that have previously been associated with increases in carbon burial and primary productivity that likely resulted in a ca. 40% abrupt decrease in atmospheric pCO_2 (from ca. 1,200 ppm to ca. 700 ppm) and ice sheet formation [10,16]. The Mesozoic to Cenozoic ice sheet history is partly constrained by $\delta^{18}O$ records because large (i.e., tens of meters) and rapid (< 1 Myr) global sea level fluctuations should be associated with changes in $\delta^{18}O$ values due to variations in ice volume [45,46]. The lowest sea level in the Cretaceous was associated with glacial polar conditions [12,17], based on present-day-like seawater $\delta^{18}O$ values [16,20,47], cool temperatures [7,48], and occurrence of glendonites [15,19], which together suggest that glacio-eustatic occurred at this time. Our reconstructed paleotemperatures derived from clumped isotope thermometry and calcu-

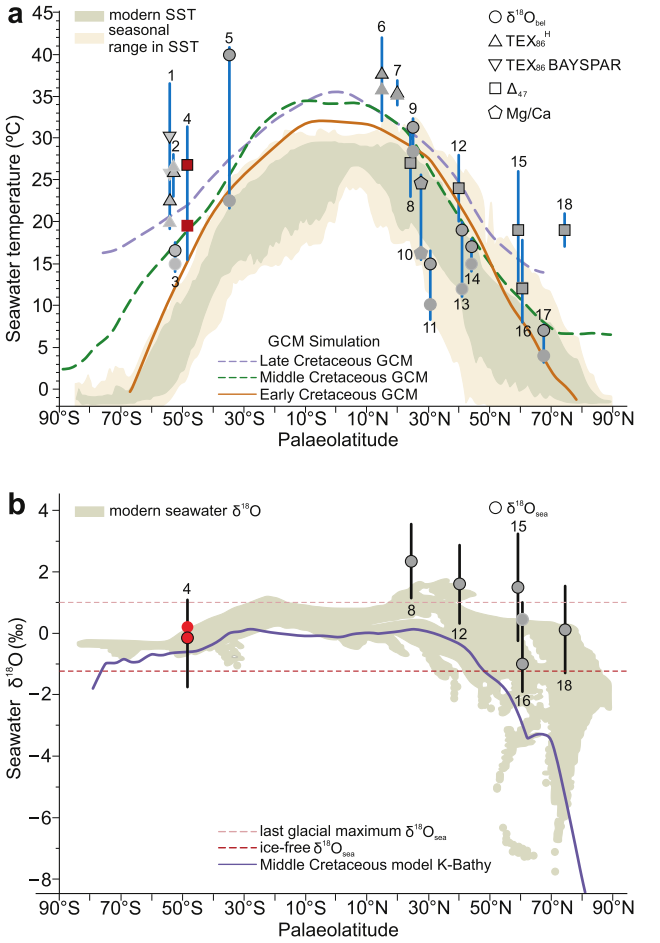

Fig. 3. Global seawater paleotemperatures and oxygen isotopic compositions in the Early Cretaceous (ca. 135 Ma). (a) Meridional seawater temperature gradients. The modern mean annual and seasonal range in seawater surface temperature (SST) observations are from the World Ocean Atlas [50]. The Valanginian temperature estimates are compared with SSTs from the Early, Middle, and Late Cretaceous general circulation model (GCM) with 4 ×, 12 ×, and 8 × pre-industrial pCO_2 values (1,120, 3,360, and 2,240 ppm), respectively [55–57]. Thick lines represent the mean seawater temperatures of the interval from pre CIE to main CIE stage I; thin lines represent the mean seawater temperatures of the interval from main CIE stage II to post CIE. Circle, square, pentagon, and triangle symbols represent other Valanginian temperature reconstructions based on multi-proxy thermometry, such as oxygen isotopes, clumped isotopes, Mg/Ca ratios, and TEX_{86} values. (1) Ocean Drilling Project (ODP) Site 692 [10]; (2) ODP Site 766 [2]; (3) ODP Site 765C [9]; (4) Gyangze (this study); (5) Deep Sea Drilling Project (DSDP) Site 167 [58]; (6) DSDP Site 603 [2]; (7) DSDP Site 534 [2]; (8) Caravaca [47]; (9) northwestern Tethys [7]; (10) Subbetic Basin [59]; (11) Vocontian Basin [16]; (12) Speeton [47]; (13) Lower Saxony Basin [36]; (14) South Boreal [8]; (15) Izhma [47]; (16) Yatria River [20]; (17) Festningen and Janusfjellet [15]; (18) Boyarka [47]. (b) Meridional seawater oxygen isotope gradients. The modern gridded mean annual $\delta^{18}O_{sea}$ data are from LeGrande & Schmidt [60]. The Valanginian $\delta^{18}O_{sea}$ (in per mil relative to VSMOW) estimates were calculated using the equation of Bernasconi et al. [31] and are compared with the modeled middle Cretaceous mean annual zonal average $\delta^{18}O_{sea}$ values [61]. Uncertainty of reconstructed temperatures and $\delta^{18}O_{sea}$ values are given as the 95% confidence level.

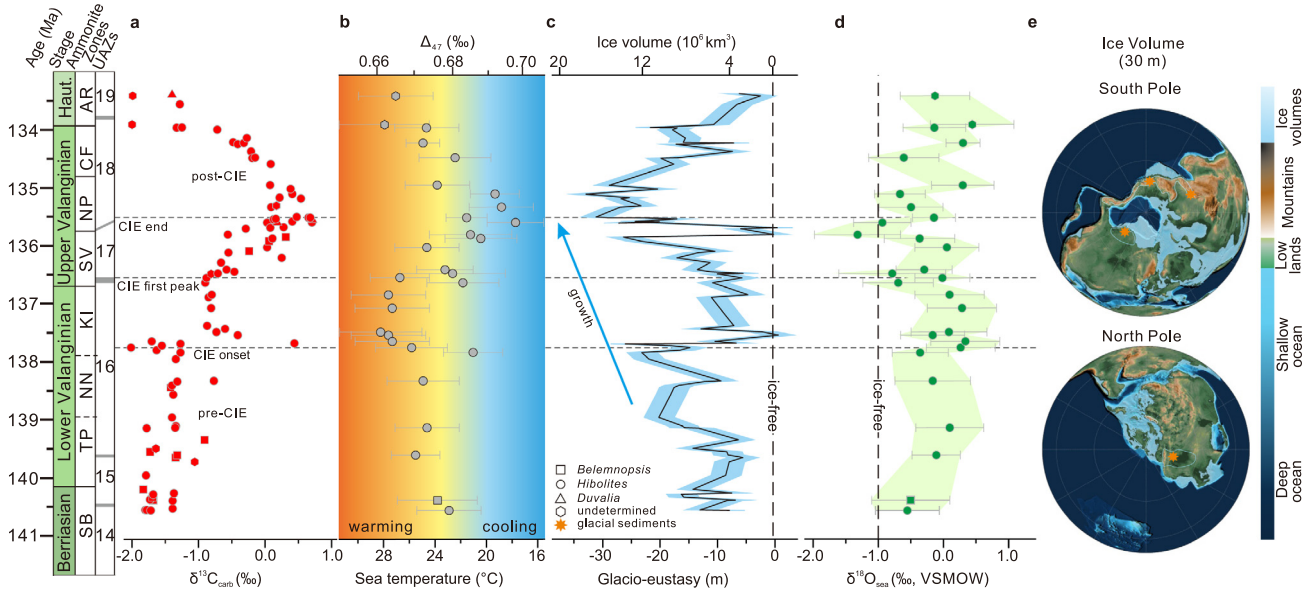

Fig. 4. Estimates of the seawater temperatures and corresponding ice sheet fluctuations in the Early Cretaceous. (a) $\delta^{13}C$ values of belemnite rostra from the Tethyan Ocean. (b) Seawater temperatures from belemnite Δ_{47} values with 95% confidence level (recalculated with the Bernasconi et al. [31] equation). (c) Belemnite $\delta^{18}O$-based sea level curve (glacio-eustatic) and ice volume trends, with 1 SD uncertainty (light blue shading), that reflect sea level changes and ice growth and decay [54] (Fig. S8; Table S3). (d) Reconstructed $\delta^{18}O_{sea}$ (‰, VSMOW) calculated using the equation of Kele et al. [30], The 95% confidence level range is shown by the light green shading and error bars. (e) Polars views of the Early Cretaceous paleogeography, which show the locations of glacial deposits [13] (blue stars) and the maximum ice volumes for 30 m of glacio-eustatic sea level change. Timescale from ref. [29].

lated $\delta^{18}O_{sea}$ data provide evidence for coupling of ocean temperatures in the Tethyan Ocean with the potential increase in ice volume, which suggests this drove climate change at mid- and southern latitudes.

To reconstruct the sea level fluctuations in deep time from the belemnite $\delta^{18}O$ data, we used isotopic data from the Eastern Tethys, which contained deeper waters that were less affected by a freshwater input. During the Early Cretaceous, seawater temperatures of 21 °C coupled with a $\delta^{18}O_{bel}$ value of −0.69‰, represent an ice-free condition. This was determined from a calculated $\delta^{18}O_{sea}$ value of −1.3‰, which is broadly equivalent to the value expected for an ice-free world (i.e., sea level of 0 m). This and the relationship between $\delta^{18}O_{bel}$ and sea level change proposed by Nordt et al. [49] allow us to reconstruct sea level fluctuations across the Valanginian interval. Applying this approach to our stratigraphic sections yields an average sea level low stand of −13 m that coincides with a positive $\delta^{18}O_{sea}$ value of −0.1‰ during the pre-CIE interval (Fig. 4). An abrupt rise in sea level may have occurred due to the increase in global seawater temperatures near the boundary with the main CIE, which is also linked to an increase in atmosphere pCO_2 [10].

After the main phase of the CIE, seawater temperatures decreased and sea level fell by 32 m, indicating the expansion of ice sheets and a return to another marine low stand for nearly 1 Myr. It is unlikely that the total ice volume during the Early Cretaceous was similar to the present-day, because of the warm mid-latitude seawater temperatures and the evidence that glacial events were limited in terms of the stratigraphy (thin deposits in thick formations) and geography (both polar regions). The present-day Antarctic ice sheet contains enough ice to change global mean sea level by 58 m [50]. Our calculated sea level change in the Early Cretaceous ranges from 0–32 m, which is equivalent to 0%–53% that of the present-day Antarctic ice sheet. The occurrence of dropstones, tillites, and glendonites in high latitude regions of both the northern and southern hemispheres suggests that Valanginian ice sheets were likely located at both poles [19,51]. Assuming an ice thickness of 1.5 km and taking into account that high-latitude regions comprise approximately 40% of the land area, we calculated an estimated ice volume of 16.5×10^6 km^3. This corresponds to an isostatically adjusted glacio-eustatic component of approximately 30 m (as shown in Figs. 4 and S8; Table S7). Our results suggest that ice may not have covered the entire land area within the polar circles. This observation is supported by the relative warmth observed in northeast Siberia, coastal Australia, and North America during this time, as indicated by the presence of continental thermophilic vegetation [8,52]. Meanwhile, recent climate modelling results suggest that potential land ice formation is limited to high-elevation regions (> 2,000 m) located in the southern and western coasts [10].

3.6. Global paleoclimatic reconstruction for the Early Cretaceous

Our reconstructed paleotemperatures derived from Δ_{47} thermometry suggest that the Valanginian CIE was characterized by climatic cooling, although a slight warming event occurred near the onset of the CIE. This global cooling trend was not interrupted by the end of the Valanginian CIE, and the coolest conditions coincided with the post-CIE interval. The proposed increase in global carbon burial, which coincided with a substantial drawdown of atmospheric pCO_2, may have contributed to ice sheet growth [10,11]. The inception of an ice sheet may be sensitive to atmospheric pCO_2, based on analogous major Phanerozoic glacial events [45,49,53]. Previous global circulation model (GCM) simulations for the Early Cretaceous indicate that small-scale continental glaciation can survive in Antarctica at pCO_2 = 840 ppm [3]. The $\Delta\delta$ ($\delta^{13}C_{carb}$–$\delta^{13}C_{plant}$)-based pCO_2 reconstruction indicates there was a ca. 40% decrease in atmospheric CO_2 levels during the Valanginian cooling event [11]. Recent climate models also support this finding, as they have revealed a decrease in atmospheric pCO_2 of 500 ppm towards the Weissert CIE end [10]. Although there are paleogeographic and climate ice sheet coupling model uncertainties, our results indicate that the existence of small- to medium- sized ice sheets (ca. $0–16 \times 10^6$ km^3; 0–30 m glacio-eustatic equivalent) required atmospheric CO_2 levels to decrease to ca. 500 ppm during the Early Cretaceous (Figs. 4 and S8; Table S7).

Recent stratigraphic and palynological investigations have shown that a cool moist climate, probably in an open sub-tundra-like set-

ting, similar to the modern taiga in northern North America, alternate with a glacial climate in Antarctica during the Early Cretaceous [19]. The present study and paleoclimatic reconstructions imply that the Early Cretaceous ice sheets were transient, and grew and decayed rapidly [3,10]. As such, estimates of the extents of the polar circles under the greenhouse conditions are more complex and variable than for the present-day polar conditions. The late Valanginian cooling interval might have been the result of enhanced nutrient influx, silicate weathering rates, organic and inorganic carbon burial, and primary productivity that led to CO_2 drawdown and subsequent global cooling [7,9,10,16]. This caused ice sheet expansion and led to the long-term, Early Cretaceous, greenhouse conditions transitioning into relatively short-lived glacial periods were preceded by warm conditions that favoured formation of widespread coal deposits or black shales [8,52] and, consequently, positive CIEs.

In contrast, the initial Valanginian glaciation was associated with little or no cooling in both the tropical and subtropical oceans, and the prevailing high seawater temperatures were not a barrier to the initiation of polar ice sheets. Previous studies have suggested that orbital dynamics during the Late Cretaceous enhanced the activity of the hydrological cycle, which may have contributed to ice sheet formation [45]. However, unlike the potential glaciation events in the extreme warmth of the Turonian [45], the late Valanginian interval was characterized by an associated global cooling trend, possibly because the cold episodes at both northern and southern high latitudes allowed ice sheet expansion. Alternatively, the growth of the ice sheets may have been due to increased sequestration of CO_2 in the deep ocean and continent, similar to the reduced oceanic upwelling during Pleistocene glacial periods [53,54]. Regardless of the exact mechanism, the temporal association of the decrease in seawater temperatures with ice sheet expansion indicates there was close coupling of the temperature of the Tethyan Ocean and polar ice volume.

4. Conclusion

By using paleoclimatic proxy records from well-preserved belemnite rostra, we show a strong coupling between Tethyan Ocean conditions and global ice volume in times of declining atmospheric carbon dioxide. Our data are derived from the continuous Cretaceous marine sediments that represent an open marine environment and contain abundant belemnite rostra, preserved in the Gyangze Basin, southern Tibet, together with more regional data. We first construct a bio-stratigraphically and chemo-stratigraphically well-constrained framework using radiolarians and strontium isotopes. We then combined carbon, oxygen and clumped isotopes with previous climate model simulations. An increase in sedimentary burial of organic carbon may have contributed to the global positive carbon isotope excursion (CIE) and have affected the total exchangeable carbon reservoir. This CIE event also led to a significant decrease in atmospheric CO_2, as testified by the cooling of 5–6 ˚C recorded in the Tethyan Ocean and the expansion of ice sheets during the late Valanginian. Belemnite $\delta^{18}O$ values suggest that sea level low stands were equivalent to ice volumes up to half of the present-day Antarctica ice sheet.

Author contributions

T.W., S.H., Q.Z. and L.D. designed research; T.W. and S.H. performed all the experiment analysis. Q.Z., G.L., F.C., C.W., J.X. and J.S. contributed to data analysis and discussion; T.W. and J.S. identified the fossils; S.H., T.W. and J.X. contributed to clumped and stable isotopic analyses; T.W., S.H., Q.Z. and Y.Y. worked on trace element testing; T.W. J.X. and S.H. performed petrographic analysis; and T.W., S.H., L.D, Q.Z. and A.F. wrote the manuscript.

Data availability

The data that support the findings of this study are included in the article and/or Supplementary materials.

Declaration of competing interest

The authors declare that they have no conflicts of interest in this work.

Acknowledgments

We thank the editors and two anonymous reviewers for their detailed and constructive comments. This work was supported by the National Natural Science Foundation of China BSCTPES project (41988101), Second Tibetan Plateau Scientific Expedition and Research Program (2019QZKK0708), the National Natural Science Foundation of China (42102021), the Chinese Academy of Sciences, Strategic Priority Research Program (XDA20070301), and the Special Research Assistant Funding Project of Chinese Academy of Sciences (2021000015).

Supplementary materials

Supplementary material associated with this article can be found, in the online version, at doi:10.1016/j.fmre.2023.05.005.

References

[1] R.A. Berner, Palaeo-CO_2 and climate, Nature 358 (1992) 114.
[2] K. Littler, S.A. Robinson, P.R. Bown, et al., High sea-surface temperatures during the Early Cretaceous Epoch, Nat. Geosci. 4 (2011) 169–172.
[3] J.B. Ladant, Y. Donnadieu, Palaeogeographic regulation of glacial events during the Cretaceous supergreenhouse, Nat. Commun. 7 (2016) 12771.
[4] E. Pucéat, C. Lécuyer, S.M.F. Sheppard, et al., Thermal evolution of Cretaceous Tethyan marine waters inferred from oxygen isotope composition of fish tooth enamels, Paleoceanography 18 (2003) 1029.
[5] C.L. O'Brien, S.A. Robinson, R.D. Pancost, et al., Cretaceous sea-surface temperature evolution: Constraints from TEX_{86} and planktonic foraminiferal oxygen isotopes, Earth Sci. Rev. 172 (2017) 224–247.
[6] S. Bodin, P. Meissner, N.M.M. Janssen, et al., Large igneous provinces and organic carbon burial: Controls on global temperature and continental weathering during the Early Cretaceous, Global Planet. Change 133 (2015) 238–253.
[7] E. Erba, A. Bartolini, R.L. Larson, Valanginian Weissert oceanic anoxic event, Geology 32 (2004) 149–152.
[8] G. Charbonnier, S. Duchamp-Alphonse, D.-F. Deconinck, et al., A global palaeoclimatic reconstruction for the Valanginian based on clay mineralogical and geochemical data, Earth Sci. Rev. 202 (2020) 103092.
[9] J. Mutterlose, M. Malkoc, S. Schouten, et al., TEX_{86} and stable $\delta^{18}O$ paleothermometry of Early Cretaceous sediments: Implications for belemnite ecology and paleotemperature proxy application, Earth Planet. Sci. Lett. 298 (2010) 286–298.
[10] L. Cavalheiro, T. Wagner, S. Steinig, et al., Impact of global cooling on Early Cretaceous high pCO_2 world during the Weissert Event, Nat. Commun. 12 (2021) 5411.
[11] D.R. Gröcke, G.D. Price, S.A. Robinson, et al., The Upper Valanginian (Early Cretaceous) positive carbon-isotope event recorded in terrestrial plants, Earth Planet. Sci. Lett. 240 (2005) 490–509.
[12] B.U. Haq, Cretaceous eustasy revisited, Global Planet. Change 113 (2014) 44–58.
[13] C.R. Scotese, An atlas of phanerozoic paleogeographic maps: The seas come in and the seas go out, Ann. Rev. Earth Planet. Sci. 49 (2021) 679–728.
[14] Á.T. Kocsis, C.R. Scotese, Mapping paleocoastlines and continental flooding during the Phanerozoic, Earth Sci. Rev. 213 (2021) 103463.
[15] G.D. Price, E.V. Nunn, Valanginian isotope variation in glendonites and belemnites from Arctic Svalbard: Transient glacial temperatures during the Cretaceous greenhouse, Geology 38 (2010) 251–254.
[16] J.M. McArthur, N.M.M. Janssen, S. Reboulet, et al., Palaeotemperatures, polar ice-volume, and isotope stratigraphy (Mg/Ca, $\delta^{18}O$, $\delta^{13}C$, $^{87}Sr/^{86}Sr$): The Early Cretaceous (Berriasian, Valanginian, Hauterivian), Palaeogeogr. Palaeoclimatol. Palaeoecol. 248 (2007) 391–430.
[17] D.C. Ray, F.S.P. van Buchem, G. Baines, et al., The magnitude and cause of short-term eustatic Cretaceous sea-level change: A synthesis, Earth Sci. Rev. 197 (2019) 102901.
[18] H.M. Stoll, D.P. Schrag, Evidence for glacial control of rapid sea level changes in the Early Cretaceous, Science 272 (1996) 1771–1774.
[19] N.F. Alley, S.B. Hore, L.A. Frakes, Glaciations at high-latitude Southern Australia during the Early Cretaceous, Aust. J. Earth Sci. 67 (2020) 1045–1095.
[20] G.D. Price, B.H. Passey, Dynamic polar climates in a greenhouse world: Evidence from clumped isotope thermometry of Early Cretaceous belemnites, Geology 41 (2013) 923–926.
[21] J. Zachos, M. Pagani, L. Sloan, et al., Trends, rhythms, and aberrations in global climate 65 Ma to present, Science 292 (2001) 686–692.

[22] K.G. Miller, M.A. Kominz, J.V. Browning, et al., The phanerozoic record of global sea-level change, Science 310 (2005) 1293–1298.
[23] J.M. Eiler, E. Schauble, 18O13C16O in Earth's atmosphere, Geochim. Cosmochim. Acta 68 (2004) 4767–4777.
[24] P. Ghosh, J. Adkin, H. Affek, et al., ^{13}C–^{18}O bonds in carbonate minerals: A new kind of paleothermometer, Geochim. Cosmochim. Acta 70 (2006) 1439–1456.
[25] A.K. Tripati, R.A. Eagle, N. Thiagarajan, et al., ^{13}C–^{18}O isotope signatures and "clumped isotope" thermometry in foraminifera and coccoliths, Geochim. Cosmochim. Acta 74 (2010) 5697–5717.
[26] J.M. Eiler, Paleoclimate reconstruction using carbonate clumped isotope thermometry, Quat. Sci. Rev. 30 (2011) 3575–3588.
[27] Y.M. Ma, T.S. Yang, W.W. Bian, et al., Early Cretaceous paleomagnetic and geochronologic results from the Tethyan Himalaya: Insight into the Neotethyan paleogeography and the India-Asia collision, Sci. Rep. 6 (2016) 21605.
[28] X.H. Li, C.S. Wang, X.M. Hu, Stratigraphy of deep-water Cretaceous deposits in Gyangze, southern Tibet, China, Cretaceous Res. 26 (2005) 33–41.
[29] J.M. McArthur, R.J. Howarth, G.A. Shields, et al., Chapter 7-Strontium Isotope Stratigraphy, Geologic Time Scale 2020, Elsevier, 2020.
[30] S. Kele, S.F. Breitenbachm, E. Capezzuoli, et al., Temperature dependence of oxygen- and clumped isotope fractionation in carbonates: A study of travertines and tufas in the 6–95 °C temperature range, Geochim. Cosmochim. Acta 168 (2015) 172–192.
[31] S.M. Bernasconi, I.A. Müller, K.D. Bergmann, et al., Reducing uncertainties in carbonate clumped isotope analysis through consistent carbonate-based standardization, Geochem. Geophys. Geosyst. 19 (2018) 2895–2914.
[32] M.L. Vickers, A. Fernandez, S.P. Hesselbo, et al., Unravelling Middle to Late Jurassic palaeoceanographic and palaeoclimatic signals in the Hebrides Basin using belemnite clumped isotope thermometry, Earth Planet. Sci. Lett. 546 (2020) 116401.
[33] R. Hoffmann, K. Stevens, The palaeobiology of belemnites-foundation for the interpretation of rostrum geochemistry, Biol. Rev. 95 (2020) 94–123.
[34] C.V. Ullmann, C. Korte, Diagenetic alteration in low-Mg calcite from macrofossils: A review, Geol. Q. 59 (2015) 3–20.
[35] D.A. Stolper, J.M. Eiler, The kinetics of solid-state isotope-exchange reactions for clumped isotopes: A study of inorganic calcites and apatites from natural and experimental samples, Am. J. Sci. 315 (2015) 363–411.
[36] P. Meissner, J. Mutterlose, S. Bodin, Latitudinal temperature trends in the northern hemisphere during the Early Cretaceous (Valanginian–Hauterivian), Palaeogeogr. Palaeoclimatol. Palaeoecol. 424 (2015) 17–39.
[37] A. Bornemann, J. Mutterlose, Calcareous nannofossil and $\delta^{13}C$ records from the Early Cretaceous of the western Atlantic Ocean: Evidence for enhanced fertilization across the Berriasian–Valanginian transition, Palaios 23 (2008) 821–832.
[38] M.E. Jelby, K.K. Śliwińska, M.J. Koevoets, et al., Arctic reappraisal of global carbon–cycle dynamics across the Jurassic–Cretaceous boundary and Valanginian Weissert Event, Palaeogeogr. Palaeoclimatol. Palaeoecol. 555 (2020) 109847.
[39] J. Mutterlose, P. Alsen, Y. Iba, et al., Palaeobiogeography and palaeoecology of Early Cretaceous belemnites from the northern high latitudes, P. Geologist. Assoc. 131 (2020) 278–286.
[40] S. Westermann, K.B. Föllmi, T. Adatte, et al., The Valanginian $\delta^{13}C$ excursion may not be an expression of a global oceanic anoxic event, Earth Planet. Sci. Lett. 290 (2010) 118–131.
[41] B. van de Schootbrugge, K.B. Föllmi, L.G. Bulot, et al., Paleoceanographic changes during the Early Cretaceous (Valanginian–Hauterivian): Evidence from oxygen and carbon stable isotopes, Earth Planet. Sci. Lett. 181 (2000) 15–31.
[42] C. Morales, A. Kujau, U. Heimhofer, et al., Palaeoclimate and palaeoenvironmental changes through the onset of the Valanginian carbon-isotope excursion: Evidence from the Polish Basin, Palaeogeogr. Palaeoclimatol. Palaeoecol. 426 (2015) 183–198.
[43] F.J. Eling, J. Gottschalk, K.D. Doeana, et al., Archaeal lipid biomarker constraints on the Paleocene–Eocene carbon isotope excursion, Nat. Commun. 10 (2019) 4519.
[44] D. Bajnai, W.F. Guo, C. Spötl, et al., Dual clumped isotope thermometry resolves kinetic biases in carbonate formation temperatures, Nat. Commun. 11 (2020) 4005.
[45] A. Bornemann, R.D. Norris, O. Friedrich, et al., Isotopic evidence for glaciation during the Cretaceous supergreenhouse, Science 319 (2008) 189–192.
[46] G.D. Price, The evidence and implications of polar ice during the Mesozoic, Earth Sci. Rev. 48 (1999) 183–210.
[47] G.D. Price, D. Bajnai, J. Fiebig, Carbonate clumped isotope evidence for latitudinal seawater temperature gradients and the oxygen isotope composition of Early Cretaceous seas, Palaeogeogr. Palaeoclimatol. Palaeoecol. 552 (2020) 109777.
[48] M.L. Vickers, G.D. Price, R.M. Jerrett, et al., The duration and magnitude of Cretaceous cool events: Evidence from the northern high latitudes, Geol. Soc. Am. Bull. 131 (11–12) (2019) 1979–1994.
[49] L. Nordt, D. Breecker, J. White, Jurassic greenhouse ice-sheet fluctuations sensitive to atmospheric CO_2 dynamics, Nat. Geosci. 15 (2022) 54–59.
[50] R.A. Locarnini, A.V. Mishonov, J.I. Antonov, et al., World ocean atlas 2013, Temperature 1 (2013) S. Levitus, Ed.; A. Mishonov, Technical Ed.;NOAA Atlas NESDIS 73, 40 pp. publication doi:10.7289/V55X26VD, dataset doi:10.7289/V5F769GT.
[51] S.E. Grasby, G.E. McCune, B. Beauchamp, et al., Lower Cretaceous cold snaps led to widespread glendonite occurrences in the Sverdrup Basin, Canadian High Arctic, Geol. Soc. Am. Bull. 129 (7–8) (2017) 771–787.
[52] W.W. Hay, S. Floegel, New thoughts about the Cretaceous climate and oceans, Earth Sci. Rev. 115 (2012) 262–272.
[53] T.J. Leutert, A. Auderset, A. Martínez-García, et al., Coupled Southern Ocean cooling and Antarctic ice sheet expansion during the middle Miocene, Nat. Geosci. 13 (2020) 634–639.
[54] I.P. Montañez, C.J. Poulsen, The Late Paleozoic ice age: An evolving paradigm, Ann. Rev. Earth Planet. Sci. 41 (2013) 24.1–24.28.
[55] D.J. Lunt, A. Farnsworth, C. Loptson, et al., Palaeogeographic controls on climate and proxy interpretation, Clim. Past 12 (2016) 1181–1198.
[56] C.J. Poulsen, D. Pollard, T.S. White, General circulation model simulation of the $\delta^{18}O$ content of continental precipitation in the Middle Cretaceous: A model proxy–comparison, Geology 35 (2007) 199–202.
[57] Y. Donnadieu, E. Puceat, M. Moiroud, et al., A better-ventilated ocean triggered by Late Cretaceous changes in continental configuration, Nat. Commun. 7 (2016) 10316.
[58] T.B. Coplen, S.O. Schlanger, Oxygen and carbon isotope studies of carbonate sediments from site 167. Magellan Rise, Leg 17, Init. Rep. Deep Sea Drill. Proj. 17 (1973) 505–509.
[59] G.D. Price, N.M.M. Janssen, M. Martinez, et al., A high-resolution belemnite geochemical analysis of Early Cretaceous (Valanginian–Hauterivian) environmental and climatic perturbations, Geochem. Geophys. Geosyst. 19 (2018) 3832–3843.
[60] A.N. LeGrande, G.A. Schmidt, Global gridded data set of the oxygen isotopic composition in seawater, Geophys. Res. Lett. 33 (2006) 1–5.
[61] J. Zhou, C.J. Poulsen, D. Pollard, et al., Simulation of modern and Middle Cretaceous marine $\delta^{18}O$ with an ocean–atmosphere general circulation model, Paleoceanography 23 (2008) PA3223.

Tianyang Wang is currently a special research assistant at the Institute of Tibetan Plateau Research, Chinese Academy of Sciences. He received the B.S. degree (2014) and Ph. D. degree (2020) in geology at the China University of Geosciences, Beijing. He is interested in biogeochemistry, global climate change, the Mesozoic paleoceanography, paleoclimate, and paleontology.

Songlin He is currently a Ph.D. candidate at the Institute of Tibetan Plateau Research, Chinese Academy of Sciences under the supervision of prof. Lin Ding. He received his B.S. degree (2017) in geology at the Chengdu University of Technology. His current research mainly focuses on the quantitative reconstruction of paleoelevation and paleoclimate of the Tibetan Plateau.

Lin Ding (BRID: 09379.00.62767) is an academician of Chinese Academy of Sciences, a full professor at the Institute of Tibetan Plateau Research, Chinese Academy of Sciences, and an honorary fellow of the Geological Society of America. His expertise lies in continental tectonics, structural geology, geochemistry and geochronology. His research interests focus on the processes of oceanic convergence and continental collision, uplift of the Tibetan Plateau, and uplift-related effects on Asian climate. He has been widely recognized as an expert with international influences and leading the study of continental collision, Tibetan Plateau uplift and environmental changes.